Atmospheric-Turbulence-Degraded Astronomical Image Restoration by Minimizing Second-Order Central Moment

Article *in* IEEE Geoscience and Remote Sensing Letters · July 2012

DOI: 10.1109/LGRS.2011.2178016

CITATIONS
28

READS
217

5 authors, including:

Houzhang Fang
Xidian University
30 PUBLICATIONS **729** CITATIONS

SEE PROFILE

Atmospheric-Turbulence-Degraded Astronomical Image Restoration by Minimizing Second-Order Central Moment

Luxin Yan, Mingzhi Jin, Houzhang Fang, Hai Liu, and Tianxu Zhang

***Abstract*—Atmospheric turbulence affects imaging systems by virtue of wave propagation through a medium with a nonuniform index of refraction. It can lead to blurring in images acquired from a long distance away. In this letter, it is observed that blurring increases the second-order central moment (SOCM) of images, and we introduce a new parametric blur identification method by minimizing SOCM. The method applies to finite-support images, in which the scene consists of a finite-extent object against a uniformly black, gray, or white background. The SOCM method has been validated by direct comparisons with other methods on simulated and real degraded images.**

***Index Terms*—Atmospheric turbulence, blur identification, image restoration, second-order central moment (SOCM).**

I. Introduction

ATMOSPHERIC turbulence severely limits the effective resolution of astronomical images that are obtained by uncompensated ground-based or space-based telescopes. The restoration of astronomical images has been actively studied [1]. Assuming that the degraded process is linear and spatially shift invariant, the degraded image g can be described as the convolution of the original noise-free blur-free image f with the point spread function (PSF) h, and an additive noise n. Therefore

$$g = h * f + n \tag{1}$$

where "$*$" denotes 2-D convolution. The goal of restoration is to seek the best estimate of f and h from the noisy degraded image g. From the refraction index structure functions, Hufnagel and Stanley [2] derived a long-exposure optical transfer function

$$H(u,v) = e^{-\lambda(u^2+v^2)^{5/6}} \tag{2}$$

to model the PSF of turbulence effect in optical imaging. Here, u and v are the horizontal and vertical frequency variables, respectively, and λ parameterizes the severity of the blur and is unknown in practice. In such situations, restoration can be formulated as blur identification and deconvolution problem since the functional form of the blur is known but the parameter is not given.

Here, the problem is stated as follows. Let us use $\hat{f}(\lambda)$ to denote the restored image with the parameter λ. Given the set $\{\Psi : \hat{f}(\lambda)|\lambda \in \Omega\}$, the question that we are interested in is which restoration should we choose. The problem is easy if f is available and one can use the peak signal-to-noise ratio (PSNR) as a measurement. The one with the maximum PSNR is the best one. However, f is not available. Two related methods for blur identification include generalized cross-validation (GCV) [3] and kurtosis minimization (KM) [4]. Both methods assume an underlying parametric model for the PSF, perform multiple deconvolutions with different PSF parameters, and choose the PSF which leads to the minimization of the GCV prediction error in [3] or the kurtosis of the restored image in [4].

Image moments are often employed to construct invariants for object recognition [5]–[7]. Zhang's previous work [8] has reported that the Gaussian blurring increases the second-order central moment (SOCM) of images, which was first defined by Hu [5]. In this letter, we mathematically prove that general types of blur do increase the SOCM of images, and thus, SOCM can be chosen as a useful criterion for selecting the best deblurred image. Based on this observation, we propose the SOCM-minimization-based blur identification method and compare it with GCV- and KM-based methods.

The remainder is organized as follows. In Section II, the relationship between blurring and SOCM is validated by mathematical derivation. The SOCM-based blur identification algorithm is reviewed in Section III. In Section IV, comparative experimental results are reported. Some concluding remarks and limitation of the method are in Section V.

II. Property of SOCM

The 2-D $(p+q)$th-order central moment $\mu_{pq}^{(f)}$ of the image $f(x,y)$ is defined as

$$\mu_{pq}^{(f)} = \iint_{R^2} \left(x - x_0^{(f)}\right)^p \left(y - y_0^{(f)}\right)^q f(x,y)\,dx\,dy \tag{3}$$

where $(x_0^{(f)}, y_0^{(f)})$ are the coordinates of the center of gravity of the image $f(x,y)$. For finite-support images, $f(x,y)$ are supposed to be piecewise continuous and nonzero only on bounded supports, i.e., $\mu_{00}^{(f)} = \int\int_{R^2} f(x,y)dxdy > 0$.

Manuscript received April 21, 2011; revised September 6, 2011 and November 9, 2011; accepted November 17, 2011. Date of publication January 23, 2012; date of current version May 7, 2012. This work was supported by the Project of the National Natural Science Foundation of China under Grants 60736010 and 60902060.

The authors are with the National Key Laboratory of Science and Technology on Multispectral Information Processing, Institute for Pattern Recognition and Artificial Intelligence, Huazhong University of Science and Technology, Wuhan 430074, China (e-mail: yanluxin@gmail.com).

Color versions of one or more of the figures in this paper are available online at http://ieeexplore.ieee.org.

Digital Object Identifier 10.1109/LGRS.2011.2178016

The $(p+q)$th-order normalized central moment $I_{pq}^{(f)}$ of the image $f(x,y)$ is defined as

$$I_{pq}^{(f)} = \frac{\mu_{pq}^{(f)}}{\mu_{00}^{(p+q+2)/2}}. \tag{4}$$

Hu [5] constructed the SOCM ϕ_1 of the image $f(x,y)$ as

$$\phi_1^{(f)} = I_{20}^{(f)} + I_{02}^{(f)}. \tag{5}$$

In what follows, we will analyze how blurring changes ϕ_1. For simplicity, we first consider the noise-free version of model (1). Generally, the degradation system is assumed to be energy preserving, i.e.,

$$\iint_{R^2} h(x,y)\,dx\,dy = 1 \tag{6}$$

and the PSF is assumed to be centrally symmetric. The assumption of centrosymmetry is not a significant limitation. Most types of blurs, such as long-term atmospheric turbulence blur and out-of-focus blur, have the PSF with a certain degree of symmetry [7]. It is easy to prove

$$x_0^{(g)} = x_0^{(f)} = x_0, \quad y_0^{(g)} = y_0^{(f)} = y_0, \quad \mu_{00}^{(g)} = \mu_{00}^{(f)} = \mu_{00}.$$

After blur, the moment of the blurred image

$$\phi_1^{(g)} = I_{20}^{(g)} + I_{02}^{(g)} = \frac{\mu_{20}^{(g)} + \mu_{02}^{(g)}}{\left(\mu_{00}^{(g)}\right)^2}. \tag{7}$$

Thereinto

$$\begin{aligned}
\mu_{20}^{(g)} &= \iint_{R^2} \left(x - x_0^{(g)}\right)^2 (f(x,y) * h(x,y))\,dx\,dy \\
&= \iint_{R^2} (x-x_0)^2 \left[\iint_{R^2} h(s,t) f(x-s, y-t)\,ds\,dt\right] dx\,dy \\
&= \iint_{R^2} h(s,t) \left[\iint_{R^2} (x-x_0)^2 f(x-s, y-t)\,dx\,dy\right] ds\,dt \\
&= \mu_{20}^{(f)} + 2\mu_{10}^{(f)} \iint_{R^2} s h(s,t)\,ds\,dt + \mu_{00} \iint_{R^2} s^2 h(s,t)\,ds\,dt \\
&= \mu_{20}^{(f)} + \mu_{00} \iint_{R^2} s^2 h(s,t)\,ds\,dt.
\end{aligned}$$

Similarly

$$\mu_{02}^{(g)} = \mu_{02}^{(f)} + \mu_{00} \iint_{R^2} t^2 h(s,t)\,ds\,dt$$

so

$$\begin{aligned}
\phi_1^{(g)} &= I_{20}^{(g)} + I_{02}^{(g)} = \frac{\mu_{20}^{(g)} + \mu_{02}^{(g)}}{\left(\mu_{00}^{(g)}\right)^2} \\
&= \phi_1^{(f)} + \frac{1}{\mu_{00}} \iint_{R^2} (s^2 + t^2) h(s,t)\,ds\,dt
\end{aligned} \tag{8}$$

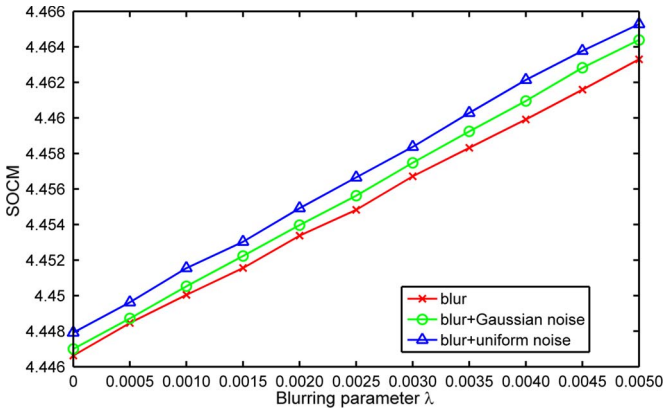

Fig. 1. SOCMs of the blurred and noisy image increase with the blur levels.

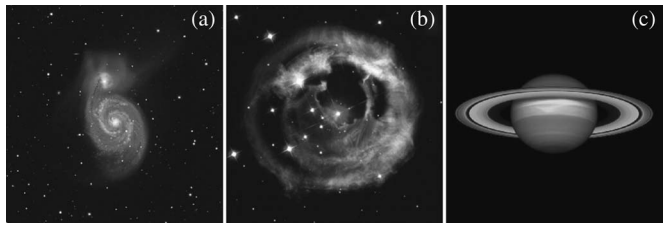

Fig. 2. Astronomical images for test. (a) M51 [10]. (b) Light echoes [11]. (c) Saturn [12]. The scales of images were adjusted for the fit display.

due to $\int\int_{R^2}(s^2+t^2)h(s,t)dsdt > 0$; thus, $\phi_1^{(g)} > \phi_1^{(f)}$, i.e., blurring increases the SOCM, and the blurred image has higher SOCM than the original image.

Furthermore, we consider the effect of additive zero-mean random noise $n(x,y)$ on SOCM. Since the image $g(x,y)$ is then a random field, all its moments and all invariants can be viewed as random variables. It holds that

$$\begin{aligned}
E\left(\mu_{pq}^{(n)}\right) &= E\left(\iint_{R^2} x^p y^q n(x,y)\,dx\,dy\right) \\
&= \iint_{R^2} x^p y^q E\left(n(x,y)\right)\,dx\,dy = 0 \\
E\left(\mu_{pq}^{(g)}\right) &= E\left(\mu_{pq}^{(f*h)}\right) + E\left(\mu_{pq}^{(n)}\right) = \mu_{pq}^{(f*h)}
\end{aligned} \tag{9}$$

where $E(X)$ denotes the mean value of the random variable X.

In practice, however, only a single image $g(x,y)$ (i.e., only one realization of a random field) is available in most cases. We obtain $\mu_{pq}^{(g)}$, but we are not able to estimate the mean values $E(\mu_{pq}^{(g)})$. Since the moments are computed by summation over the whole image, they should be affected very little by additive zero-mean noise [6], [7]. For nonzero-mean random noise, (9) does not hold right any longer. Consequently, the proposed method may become invalid.

Fig. 1 shows how blurring changes the SOCM of the blurred and noisy images. The image shown in Fig. 2(b) is blurred by atmospheric turbulence blur. The blurring parameter λ varies from 0 to 0.005 in increments of 0.0005, and additive zero-mean Gaussian and uniform random noise are added at blurred signal-to-noise ratio (BSNR) of 40 dB. BSNR is defined here as

$$\text{BSNR} = 10\log_{10}\left(\frac{\text{variance of } h*f}{\text{variance of } n}\right). \tag{10}$$

It is evident that the SOCMs of the blurred and noisy image increase with the blur levels. Moreover, the presence of the zero-mean random noise does not change the SOCM values significantly. Therefore, the blurred and noisy image has higher SOCM than the original image. Benefiting from this regular property, SOCM can be chosen as a useful criterion for estimating the optimal blurring parameter in the presence of noise.

III. SOCM Minimization for Blur Identification

Giving a noisy blurred image g with a parametric form for the PSF, we estimate the blur parameter λ. The search space Ω is set manually on a trial-and-error basis. If the upper limit of λ is too large, then the corresponding restored image would be very degraded. In actual applications, the long-exposure atmospheric turbulence blurring parameter can be roughly pre-estimated by visual inspection [9]. It is advisable to select an overestimation of the parameter as the upper limit. At each step in the search loop, the image is deblurred using a Wiener filter or any other nonblind restoration algorithm, and the SOCM of the deblurred image $\hat{f}(\lambda)$ is computed and recorded. Then, the deblurred image with the minimal SOCM is chosen as the final restored image, and the corresponding λ^* is regarded as the identified blurring parameter. The SOCM-based blur identification can be formulated as

$$\lambda^* = \arg\left\{\min_{\lambda\in\Omega} \phi_1\left(\hat{f}(\lambda)\right)\right\}. \tag{11}$$

The nonblind restoration algorithm used in this letter is the practical form of the Wiener filter

$$\hat{F}(u,v) = \frac{H^*(u,v)}{|H(u,v)|^2 + nsr} G(u,v) \tag{12}$$

where G, H, and $\hat{F}$ denote the Fourier transform of g, h, and $\hat{f}$, respectively, H^* is the conjugate of H, and nsr is the noise-to-signal ratio, which can be approximated by the noise-to-blurred-signal ratio. In this letter, nsr is approximately calculated from the blurred image by the ratio of the noise variance and the signal variance. Since the image is limited to be composed of a finite-extent object against a uniform background, we estimate the noise variance from the object region and the signal variance from the background region. The noise variance is approximated by the average variance of the several local regions selected from the background. The signal variance is approximated by the maximum variance of the several local regions selected from the object region.

IV. Experiments on Real and Simulated Atmospheric Turbulence Blurred Images

Several test images, as shown in Fig. 2, were selected for the simulated experiments. The test images were blurred with $\lambda = 0.001$, 0.002, and 0.003 to simulate the effects of varying degrees of turbulence blur. Gaussian noise was added at levels of 40–70-dB BSNR at intervals of 5 dB.

SOCM, KM, and GCV methods were tested, and λ search space was set as $\Omega = \{\lambda : 0.0001i | i = 0, 1, \cdots, 40\}$. Both GCV and KM methods also used the Wiener filter for restoration. Since the ground-truth images are available, the PSNR can be used to measure the quality of the restored images. PSNR is defined as

$$\text{PSNR} = 10\log_{10} \frac{\sum_{i=1}^{M}\sum_{j=1}^{N} 255^2}{\sum_{i=1}^{M}\sum_{j=1}^{N}\left(f(i,j) - \hat{f}(i,j)\right)^2} \tag{13}$$

where $M \times N$ is the image size. Then, the PSNR and λ of the degraded (BSNR = 60 dB, varying degrees of turbulence blur) and the restored images by the three methods are summarized in Table I. SOCM has a slightly lower PSNR on Fig. 2(b) (blurred with $\lambda = 0.003$). For all other images, SOCM results are the best. In most cases, the SOCM method also obtains more accurate estimates of the actual blur parameter.

Moreover, the effects of noise were investigated. For the three methods, the PSNR of the restored image versus varying noise levels on the simulated degraded image of Fig. 2(c) (blurred with $\lambda = 0.002$) was plotted in Fig. 3. In every case, the SOCM method has achieved the highest PSNR among the three methods.

TABLE I
PSNR (in Decibels) and Identified λ Comparisons of the Three Methods for the Test Images (BSNR = 60 dB; the First Row Is PSNR, and the Second Is λ)

image	degraded image	image restored by SOCM	KM	GCV
Fig. 2a	34.01	**39.08**	33.55	26.69
	0.001	0.0011	0.0016	0.0017
	31.14	**37.42**	36.91	30.37
	0.002	0.0022	0.0024	0.0027
	29.67	**33.20**	32.58	32.06
	0.003	0.0041	0.0043	0.0036
Fig. 2b	30.39	**34.62**	31.84	33.17
	0.001	0.0010	0.0015	0.0011
	28.99	**31.56**	30.04	31.01
	0.002	0.0023	0.0030	0.0016
	28.39	29.30	29.03	**29.41**
	0.003	0.0045	0.0048	0.0019
Fig. 2c	33.64	**40.70**	33.80	30.86
	0.001	0.0012	0.0016	0.0015
	30.59	**38.54**	38.08	35.35
	0.002	0.0021	0.0018	0.0023
	29.08	**36.46**	35.54	36.12
	0.003	0.0033	0.0031	0.0030

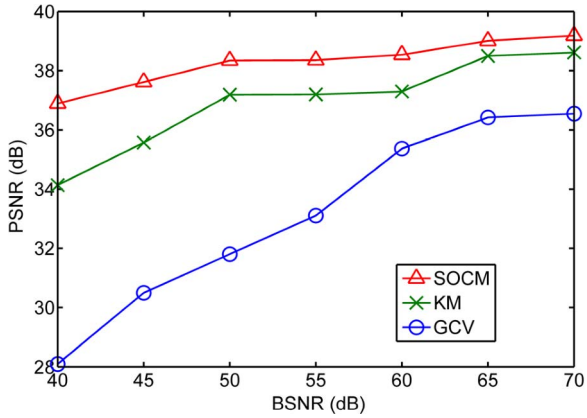

Fig. 3. PSNR of restored image versus BSNR level for simulated degraded image of Fig. 2(c) (blurred with $\lambda = 0.002$) by the three methods (SOCM, KM, and GCV).

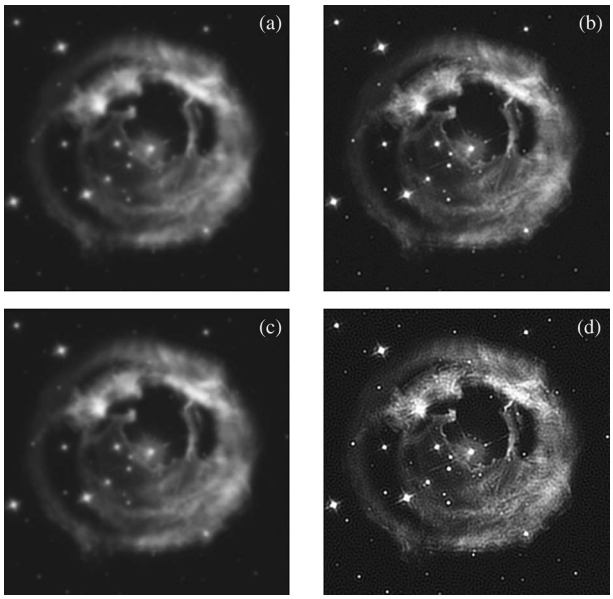

Fig. 4. Restoration of a simulated degraded image. (a) Simulated degraded image (PSNR = 31.12 dB, BSNR = 40 dB, and $\lambda = 0.002$). Restored image by (b) SOCM (PSNR = 35.89 dB and identified $\lambda = 0.0023$), (c) KM (PSNR = 31.24 dB and identified $\lambda = 0.0001$), and (d) GCV (PSNR = 27.34 dB and identified $\lambda = 0.0031$).

TABLE II
CALCULATING TIME OF THE GCV AND SOCM METHODS ON SIMULATED DATA

image	GCV	SOCM
Fig. 2a (512×512)	552.4s	5.9s
Fig. 2b (300×300)	190.6s	1.8s
Fig. 2c (800×400)	664.1s	6.6s

Fig. 4 shows an example of restoration for a BSNR of 40 dB and a parameter λ of 0.002. The λ identified by KM is 0.0001, far less than the actual one, and the result image [see Fig. 4(c)] appears to be "underdeblurred." GCV identified it as 0.0031, the restored image [see Fig. 4(d)] appears to be "overdeblurred," and the noise is amplified. SOCM identified it as 0.0023 and obtained reliable identification and restoration results [see Fig. 4(b)]. The GCV method seems to be more sensitive to noise. This is because the GCV criterion is built on the data itself and susceptible to noise. Both SOCM and KM are based on the statistical characteristics of the image and thus are less sensitive to noise. These experimental results show that the SOCM method is superior for blur parameter identification at a wide range of noise levels.

Furthermore, the calculating time of the GCV and SOCM methods on simulated data is listed in Table II. The tests are performed in MATLAB 2008a, on a personal computer with a 2.93-GHz CPU and 2-GB memory. In practice, for the KM method, because the whole image often does not follow the kurtosis statistic stated in [4], one has to manually search the subimages that follow the kurtosis statistic. It is time consuming and difficult to calculate the time cost. Thus, the calculating time of the KM method is not listed. The SOCM has the lowest computational load among the three methods, which makes the method more preferable in actual applications.

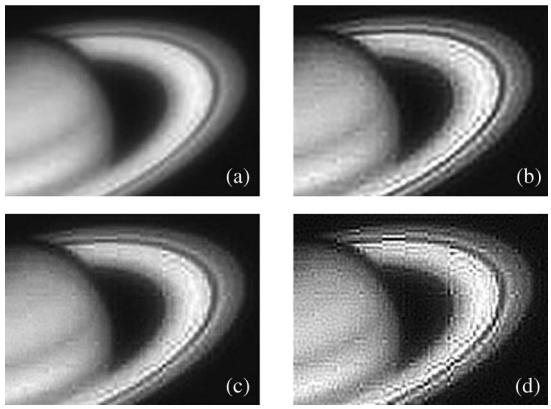

Fig. 5. Restoration close-ups of a real degraded image. (a) Real degraded image [11]. Restored image by (b) SOCM (identified $\lambda = 0.0013$), (c) KM (identified $\lambda = 0.0007$), and (d) GCV (identified $\lambda = 0.0011$).

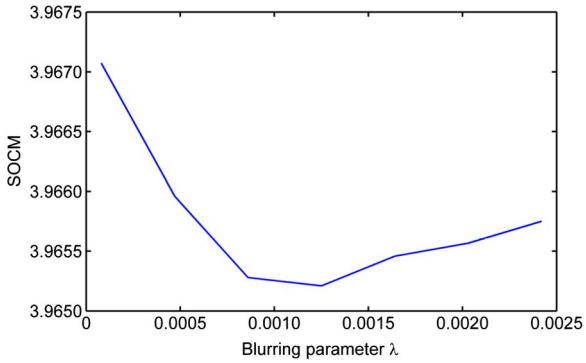

Fig. 6. SOCM profile as a function of λ.

An example of a real degraded image is shown in Fig. 5 [12]. The size of the image is 400 by 400. The λ search space was set as $\Omega = \{\lambda : 0.0001i | i = 0, 1, \ldots, 25\}$. For convenience of comparison, the partial close-ups are displayed. Obviously, more fine details are restored in Fig. 5(b) by SOCM. Fig. 6 shows that the SOCM profile of the entire real image is concave. The KM-restored result [see Fig. 5(c)] appears to be "underdeblurred." The GCV-restored result [see Fig. 5(d)] contains many artifacts and looks unnatural. Among the three methods, SOCM has the lowest computational complexity. SOCM took 2 s while GCV took 114 s on a personal computer with a 2.93-GHz CPU and 2-GB memory.

V. CONCLUSION

In conclusion, a new blur identification and restoration method by minimizing SOCM is presented. It is based on the observation that blurring increases the SOCM of images. We mathematically analyzed the observed property of SOCM. Its application in restoring astronomical images degraded by atmospheric turbulence is highlighted. Comparisons with other methods suggest that the SOCM method is competitive in restoring astronomical images degraded by atmospheric turbulence blur. The method is limited to finite-support images and can be further applied in medical imaging and microscopy imaging.

ACKNOWLEDGMENT

The authors would like to thank Prof. S. J. Reeves of the Electrical and Computer Engineering Department, Auburn University, for providing MATLAB codes of the GCV method and the reviewers for their valuable and helpful suggestions.

REFERENCES

[1] R. Molina, J. Nunez, F. J. Cortijo, and J. Mateos, "Image restoration in astronomy: A Bayesian perspective," *IEEE Signal Process. Mag.*, vol. 18, no. 2, pp. 11–29, Mar. 2001.

[2] R. E. Hufnagel and N. R. Stanley, "Modulation transfer function associated with image transmission through turbulent media," *J. Opt. Soc. Amer. A, Opt. Image Sci.*, vol. 54, no. 1, pp. 52–60, Jan. 1964.

[3] S. J. Reeves and R. M. Mersereau, "Blur identification by the method of generalized cross-validation," *IEEE Trans. Image Process.*, vol. 1, no. 3, pp. 301–311, Jul. 1992.

[4] D. Li and S. Simke, "Atmospheric turbulence degraded image restoration by kurtosis minimization," *IEEE Geosci. Remote Sens. Lett.*, vol. 6, no. 2, pp. 244–247, Jul. 2009.

[5] M. K. Hu, "Visual pattern recognition by moment invariants," *IRE Trans. Inf. Theory*, vol. 8, no. 2, pp. 179–187, Feb. 1962.

[6] T. Suk and J. Flusser, "Combined blur and affine moment invariants and their use in pattern recognition," *Pattern Recognit.*, vol. 36, no. 12, pp. 2895–2907, Dec. 2003.

[7] J. Flusser, T. Suk, and S. Saic, "Image features invariant with respect to blur," *Pattern Recognit.*, vol. 28, no. 11, pp. 1723–1732, Nov. 1995.

[8] T. X. Zhang and J. Liu, "Investigation on the stability of object moment invariants," (in Chinese), *J. Infrared Millim. Waves*, vol. 23, no. 3, pp. 197–200, Jun. 2004.

[9] R. C. Gonzalez and R. E. Woods, *Digital Image Processing*, 2nd ed. Upper Saddle River, NJ: Prentice-Hall, 2002.

[10] [Online]. Available: www.astrosurf.com/re/ultra-deep-m51.html

[11] [Online]. Available: http://www.cmnh.org/site/AtTheMuseum/PlanetariumandObservatory/AstronomyLectures.aspx

[12] [Online]. Available: http://en.wikipedia.org/wiki/saturn

[13] [Online]. Available: http://sse.jpl.nasa.gov/multimedia/display.cfm?IM_ID_131